Making superior corrosion resistant aluminum oxide films using ozone-electrochemical and electron microscopy studies

A. Kuznetsova, I. Popova, V. Zhukov, and J. T. Yates, Jr.[a)]
Surface Science Center, Department of Chemistry, University of Pittsburgh, Pittsburgh, Pennsylvania 15260

G. Zhou and J. C. Yang
Materials Science and Engineering Department, University of Pittsburgh, Pittsburgh, Pennsylvania 15261

X. Chen
Materials Science Division, Argonne National Laboratory, Argonne, Illinois 60439

(Received 9 October 2000; accepted 5 February 2001)

Aluminum surfaces have been subjected to oxidation at 300 K, using a molecular beam of ozone of 97% purity. An enhancement of the kinetics of oxidation is found compared to oxidation by O_2. The oxide film produced exhibits enhanced corrosion resistance as measured by several electrochemical methods compared to comparable thickness oxide films made by oxygen exposure. Transmission electron microscopy measurements show that the ozone-grown films exhibit small pore sizes and also increased average density as measured by the behavior of the radial distribution function derived from electron diffraction measurements on films made from ozone and oxygen. These effects may be due to the lower oxygen vacancy defect density in films made from ozone. The special properties of ozone-grown aluminum oxide films are preserved even after the films are removed from vacuum and exposed to the atmosphere. © *2001 American Vacuum Society.*
[DOI: 10.1116/1.1359536]

I. INTRODUCTION

The use of energetic oxygen-containing species to oxidize aluminum surfaces has been found to produce an oxide film which exhibits superior corrosion passivation properties compared to films of similar thickness produced by ordinary oxidation procedures. Thus, we have shown that electron attachment to adsorbed water molecules that produces the temporary negative ion, H_2O^- leads to fast oxidation of the Al(111) surface as well as to the production of an oxide film with superior corrosion passivation properties.[1,2] It is believed that the H_2O^- species generates a hydroxyl radical, ·OH, which is an energetic oxidizing agent.

In the same spirit, the ozone molecule, O_3, is an energetic species. The Gibbs free energy of the reaction to produce ozone from oxygen is shown in Eq. (1).

$$3/2O_2(g) \rightarrow O_3(g); \quad \Delta G^0 = 163 \text{ kJ/mol}. \tag{1}$$

The investigation of the interaction of O_3 with the Al(111) surface is reported in another paper, where x-ray photoelectron spectroscopy (XPS) was employed to investigate the kinetics of oxidation as well as the character of the oxide film produced from O_3 compared to that produced from O_2.[3]

In this article, we apply O_3 to a polycrystalline Al surface and then use a variety of probes to more fully understand the properties of the oxide film compared to films of comparable thickness which are made using O_2 as the oxidizing agent. The oxide films produced from O_3 and O_2 have been compared by electrochemical methods and also by transmission electron microscopy methods, and it has been found that O_3 produces an oxide film of higher density and smaller pore diameter than O_2, as well as superior corrosion passivation properties. A rationale involving the reduction of oxygen vacancy defects by O_3 is proposed to explain the higher corrosion passivation quality of the O_3-produced film compared to the O_2-produced film.

II. EXPERIMENT

Samples of pure polycrystalline aluminum (99.999%, Goodfellow) $1.4\times1.4\times0.15$ cm^3 were mechanically polished with SiC abrasive paper (600 grit) and then electropolished in a 1% NaOH solution for periods sufficiently long 300 C/cm^2) to remove the thick oxide layer. Then the Al samples were transferred into an ultrahigh vacuum chamber[2] and cleaned to the final stage with Ar^+ bombardment ($E_{Ar^+}=1$ keV, $P_{Ar}=5\times10^{-5}$ Torr, $I/A=8$ μA/cm^2) for 2–3 h using a Leybold IQE 10/35 ion gun. The samples were then annealed to 673 K for 5 min. The cleanliness of the Al surface was measured using an Auger electron spectrometer until, following ion bombardment and annealing, only the $Al^0(LVV)$ feature in the Auger spectrum was observed. We estimate that less than 1 at. % of oxygen was present on the cleaned surface, judging from the $O(KLL)/Al^0(LVV)$ intensity ratios which were near zero. Nine aluminum samples were oxidized using O_3 and seven were oxidized using O_2.

The ultrahigh vacuum (UHV) chamber is equipped with a 360 l/s ion pump, a 150 l/s turbopump, and a titanium sublimation pump. The base pressure measured after a 12 h bakeout was typically 2×10^{-10} Torr. Residual gas analysis was carried out with a quadrupole mass spectrometer (UTI Instruments/100C).

[a)]Electronic mail: jyates@imap.pitt.edu

An all glass ozone generator[4] was used to produce ozone from oxygen at 1 atm (99.994% pure O_2, VWSCO). Ozone produced in the high voltage capacitor tube is trapped in silica gel at 195 K using an acetone/dry ice bath. Residual oxygen was pumped away using a mechanical pump, and O_3 was then evolved from the silica gel by slight warming.

O_3 (97% pure) was supplied to the chamber through an all-glass doser assembly[5] containing a glass capillary of ~0.06 mm inner diameter to control the conductance of O_3 into the UHV chamber. Taking into account the fractional interception of the gas beam by the sample, estimated to be $\alpha=0.6$ from the doser/sample geometry,[6] the incident flux of O_3 and O_2 is, respectively, 2.7×10^{13} O_3 molecules cm^{-2} $s^{-1}\cdot[P(\text{Torr})]$ and 3.4×10^{13} O_2 molecules cm^{-2} s^{-1} $\cdot[P(\text{Torr})]$, where $P(\text{Torr})=$ pressure in the high pressure gas storage line (both O_3 and O_2 were used at ~4 Torr).

The Al samples, oxidized with either O_3 or O_2, were transferred from the UHV chamber to an electrochemical cell for electrochemical impedance spectroscopy (EIS) measurements and Tafel analysis. The conventional three-electrode electrochemical cell, described previously,[2] was used for EIS and Tafel measurements. The cell, filled with 3.5% NaCl solution, contains a counterelectrode (Pt), a reference electrode (saturated Calomel, SCE) and a working electrode (the Al sample). The electrolyte was also deaerated with nitrogen gas (N_2, 99.998%) for 30 min before the measurements.

EIS spectra were taken at open circuit potential with a potentiostat–galvanostat programmable electrochemical impedance apparatus (model PGZ301, Radiometer). The frequency range was from 100 kHz to 10^{-2} Hz. The amplitude of the applied ac potential was 5 mV in the EIS measurements.

Linear polarization measurements (Tafel analysis) were performed for two representative samples after EIS measurements using a scan rate for the potential applied to the test electrode of 0.8 mV/s. The potential was applied in the range between −1.50 and −0.66 V.

Transmission electron microscopy (TEM) analysis was employed to study the structure of the amorphous Al_2O_3 films. The microscope (JEOL200CX TEM, operated at 200 keV) is equipped with a Philips energy-dispersive x-ray (EDX) detector to perform energy dispersive x-ray spectroscopy. Digital capture of the selected area diffraction pattern (SAED) was performed to measure a radial distribution function (RDF).[7] The data acquired were described by the function, $J(r)$, which represents the number of atoms lying at distances between r and $r+dr$ from the center of an arbitrary atom. This function is proportional to the average density, ρ^0, at very large values of r where the distribution of atoms appears to be homogeneous from the center.

III. RESULTS

A. Kinetics of aluminum oxidation at 300 K

The kinetics of aluminum oxidation monitored by Auger electron spectroscopy are shown in Figs. 1 and 2. Figure 1 shows the sequence of Auger spectra obtained for oxygen and ozone exposure at 300 K. Auger spectra for the oxidation process from O_2 exposure are shown in the top part of Fig. 1 and Auger spectra for oxidation by O_3 (g) are shown in the bottom part of Fig. 1. The growth of the $Al^{3+}(LVV)$ peak at 56 eV and the O(*KLL*) feature at 525 eV and the decrease of the $Al^0(LVV)$ (68 eV) peak is observed with increasing exposure. Much more rapid oxidation is observed in the case of O_3. By an exposure of 6.4×10^{15} O_3/cm^2, the Al^0 peak completely disappears from the spectrum.

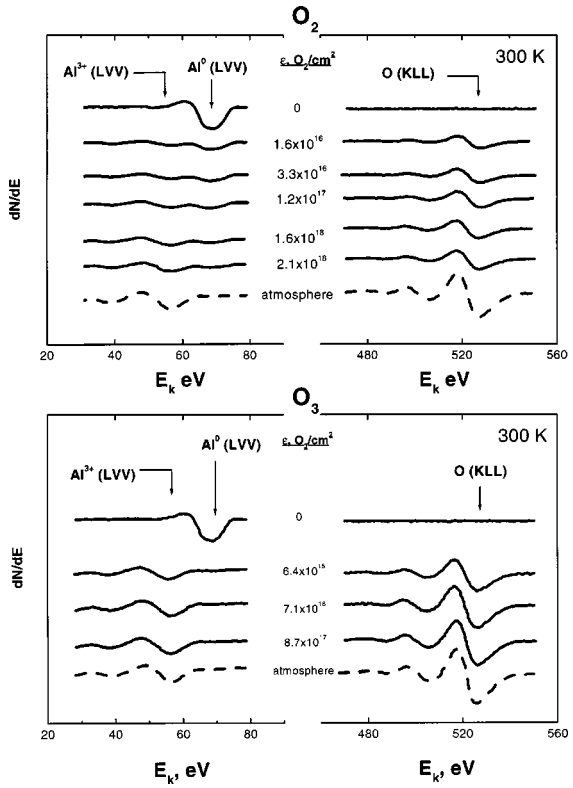

FIG. 1. Auger spectra of aluminum oxidized by O_3 and O_2 at 300 K.

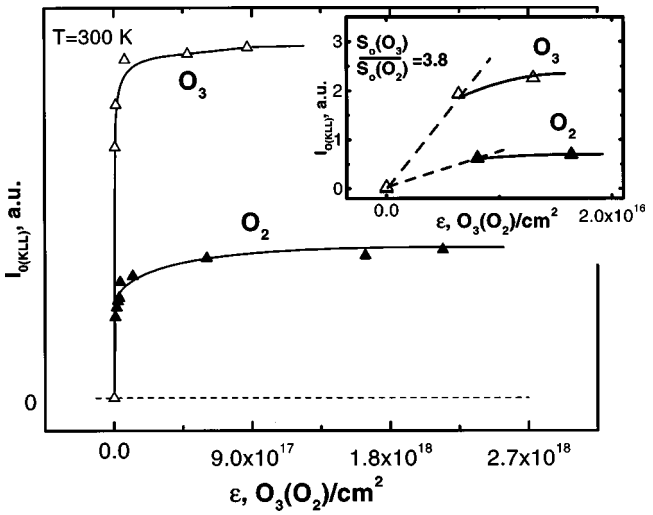

FIG. 2. Kinetics of aluminum oxidation by O_2 and O_3 measured by Auger spectroscopy. The inset shows the initial growth of the oxygen Auger intensity, and the initial slopes yield sticking coefficient, $S_o(O_3)$ and $S_o(O_2)$.

Figure 1 shows also the change in the Auger peaks when the samples were exposed to atmosphere following controlled oxidation in the vacuum system. Additional growth of the oxygen Auger peak-to-peak intensity both for ozone-formed and oxygen-formed oxides is observed upon atmospheric exposure. A 20% increase in the oxygen signal for the ozone-oxidized sample is observed after atmospheric exposure. Following atmospheric exposure the oxygen signal from the oxygen-formed oxide is 83% of the signal for the ozone-formed oxide after both oxide films were exposed to atmosphere.

Figure 2 shows the uptake curve for the O_2 and O_3 reactions with aluminum. The relative initial sticking coefficients for ozone and oxygen adsorption, evaluated by the initial slope of the oxygen signal in the Auger spectra, is shown in the inset of Fig. 2. The initial sticking coefficient for ozone is 3.8 times higher than that for oxygen.

B. Electrochemical impedance spectroscopy study and Tafel analysis of the various oxide films

EIS spectra for 16 experiments (shown at the top of Fig. 3) and Tafel plots for 2 representative samples (shown at the bottom of Fig. 3) were measured from the aluminum sample oxidized with ozone and with oxygen using the same exposure of 2.0×10^{18} O_3/cm^2 or O_2/cm^2. The change of the impedance of the cell is described by the formula

$$Z=R_s+R_o/(1+\omega R_oC)^2+j(-\omega R_o^2C)/[1+(\omega R_oC)^2], \quad (2)$$

where Z=total impedance, in Ω; R_s and R_o are the resistances of the electrolyte solution and the oxide film respectively, in Ω; C=capacitance of the oxide, in farads; $\omega=2\pi f$, where f=ac frequency, in Hz; and $j=\sqrt{-1}$.[8] The formula for the impedance, Z, was fitted to the EIS data obtained to extract the values for resistance, R_o, and capacitance, C_o, of the aluminum oxide layer.

The thickness was evaluated according to the dependency for a parallel plate capacitor with $C=\varepsilon\varepsilon_0A/d$, where C=capacitance, in farads; ε=dielectric constant; $\varepsilon_0=8.85\times10^{-12}$ F/m; A=area of the sample, in m^2; and d=thickness of the oxide, in m. Using a dielectric constant of 8.5, the calculated average thickness for the ozone-grown oxide is 15.1 Å and for the oxygen-grown oxide the average thickness is 16.0 Å.

The Tafel plot corrosion measurement method uses a wide dc potential spectrum and provides additional corrosion information (bottom of Fig. 3). The corrosion current density was evaluated using VoltaLab40 software. The ozone-formed oxide shows a corrosion current density of 48 nA/cm^2; the oxygen-formed oxide shows a corrosion current density of 216 nA/cm^2. The corrosion current density is proportional to the corrosion rate according to the dependence

$$\text{rate}_{\text{corr}}=I_{\text{corr}}\Lambda\ 1/\rho\,\varepsilon, \quad (3)$$

where I_{corr}=corrosion current density, A/cm^2; Λ=empirical constant=1.2866×10^5, (in equivalents of s mil/C cm year);

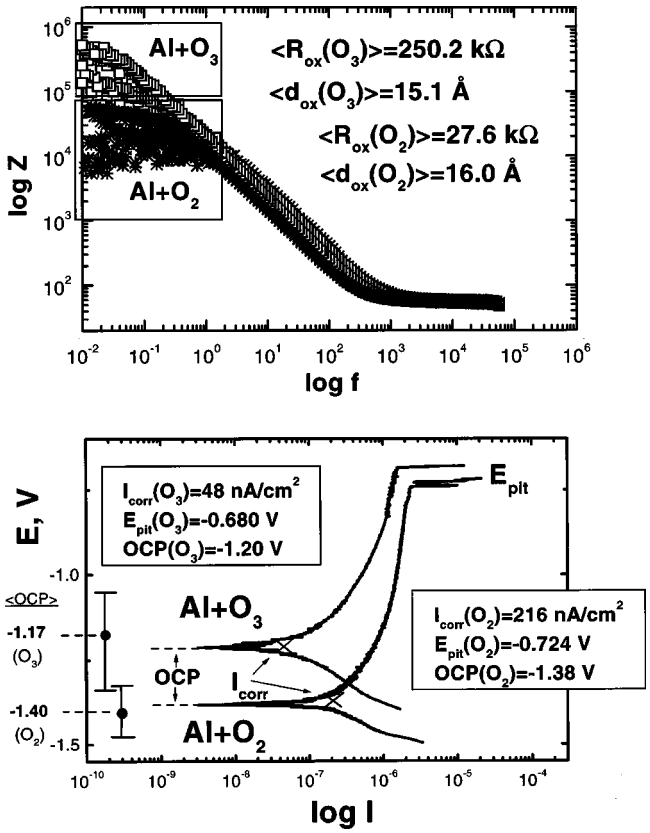

FIG. 3. Electrochemical impedance spectra of aluminum oxidized with O_2 and O_3, showing results for 16 measurements and representative Tafel plots for O_2- and O_3-oxidized samples.

ρ = metal density (in g/cm^3); ε = equivalent weight, (in g/equivalent).[8] Therefore, the rate of corrosion for the O_3-formed layer is significantly lower.

The E_{pit} (pitting potential) values for the ozone-formed oxide is higher by 44 mV, also showing superior oxide film stability toward pitting.

The open circuit potential (OCP) represents the potential for zero net current flowing through the sample. It was measured for all 16 samples after 30 min of electrolyte deaeration. The average values of the OCP and the range of the OCP for all samples studied is shown by the range bars in Fig. 3. The average OCP value for the O_3-formed oxide is -1.17 V, and for the O_2-formed oxide the OCP is -1.40 V, and the difference is significant when compared to the statistical range of the OCP measurements.

C. TEM measurements

Figure 4(a) shows a TEM image from an aluminum sample oxidized with oxygen. The bright features, postulated to be pores in the oxide structure, have a distribution in size from 30 to 700 Å, with an average pore size of 200 Å. The SAED pattern taken from this area is shown in the upper-right inset of Fig. 4(a). Figure 4(b) shows a TEM image from an aluminum sample oxidized with ozone. The inset is the

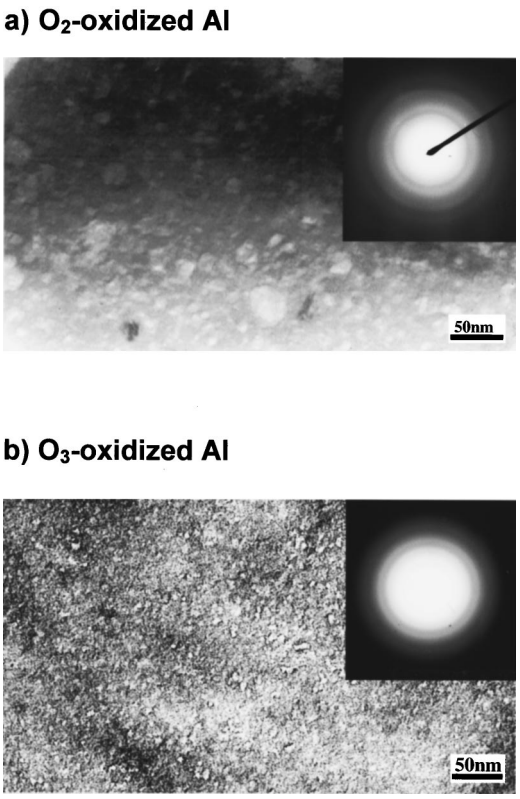

FIG. 4. TEM images of (a) an O_2-oxidized sample and an (b) O_3-oxidized sample. The insets are the electron diffraction pattern of the oxide film.

SAED pattern corresponding to this area. The range of pore diameter distribution is estimated to be from a few angströms to 100 Å, with a typical diameter of 40 Å.

Both oxides are amorphous as judged by the diffuse ring of the SAED patterns for both samples. A qualitative comparison of the diffraction patterns for the two oxide films indicate that they differ. The compositions of the two oxide films were measured by EDS, showing that both samples contain aluminum.

Figure 5 shows the function $[J(r)(O_3)-J(r)(O_2)]/J(r)\times(O_2)$ as a function of r. At large r the difference in this function represents the difference between the average densities of ozone-formed and oxygen-formed oxide, which approaches 4%.

IV. DISCUSSION

A. Surface reactivity of O_3 compared to that of O_2

It is known from the literature that the initial O_2 surface reactivity at 300 K, as judged by the sticking coefficient of O_2 molecules on the Al(111) surface, is rather low (0.005–0.02).[9a,9b] Ozone, on the other hand, is known to be highly reactive on various surfaces including noble metals. For instance, the dissociative sticking coefficient of the O_3 molecule on the Pt(111) surface at 300 K is 0.24.[10] In other studies the high reactivity of ozone was used for oxidation of silicon surfaces using ozone dissolved in water.[11] The very

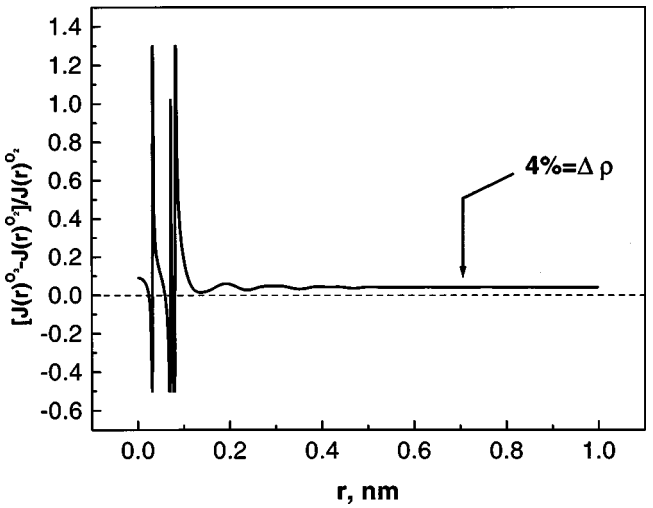

FIG. 5. Relative difference in film densities represented as $[J(r)(O_3)-J(r)(O_2)]/J(r)(O_2)$, where $J(r)$ = radial distribution function.

weak O–O bond in ozone is probably a thermodynamic factor related to its higher reactivity with the aluminum surface; $[D(O_2-O)=106.7$ kJ/mol$]$.[12]

In our study of oxidation of both the Al(111) single crystal surface[3] and polycrystalline aluminum by O_2 and O_3 molecules, a higher reactivity was measured for O_3 as well. For Al(111) at 300 K, the ratio of the initial sticking coefficients is $S_o(O_3)/S_o(O_2)=6.7$.[3] On polycrystalline Al the $S_o(O_3)/S_o(O_2)$ ratio is 3.8, as seen from Fig. 2.

For O_3 exposures above $\sim 1.3\times 10^{16}$ O_3/cm^2 a saturation effect for O_3 adsorption is observed. The rate of adsorption decreases to almost zero as seen in Fig. 2.

These results clearly show that both initial surface reactivity and saturation coverage of O_3 on both polycrystalline Al and with Al(111) exceeds that of O_2 by a large factor.

B. TEM and SAED studies of oxide morphology and density

TEM measurements revealed that both ozone- and oxygen-produced oxide films are amorphous in nature. A larger pore size and lower density for oxygen-grown oxide is observed by TEM and SAED methods. A 4% difference in the densities of O_2- and O_3-produced oxide films is derived from the radial distribution function, $J(r)$, at large values of r. Such a difference in structure can be rationalized by a schematic representation of the oxide structure, shown in Fig. 6.[13] Due to the amorphous nature of the oxide, the aluminum and oxygen ions can form irregular groups of rings. We postulate that more open rings, produced by O_2, and due to oxygen vacancy effects, are partially eliminated by O_3 oxidation.

The size of the pore channels will determine the diffusion rate of the ions and electrons and the rate of corrosion. The denser structure is expected to be more resistant to electron and ion transport. Due to its higher reactivity (as measured by the sticking coefficient), we postulate that O_3 is able to

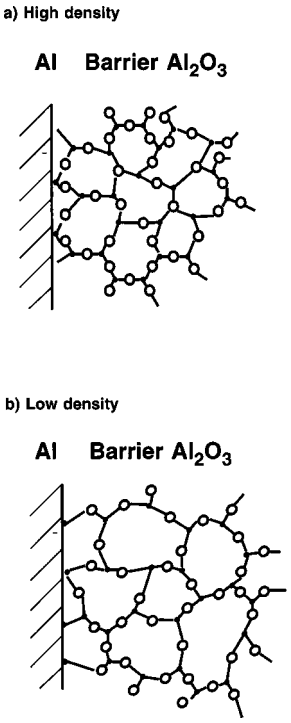

FIG. 6. Schematic two-dimensional representation of aluminum oxide structures.

reduce the density of oxygen vacancies, causing the pore size to decrease and the film density to increase. The differences in oxide film structure implied schematically in Fig. 6 at the atomic level are probably connected to the differences in pore size shown in Fig. 4 at the 10–100 Å level of measurement.

C. Electrochemical evaluation of aluminum oxide layers

The electrical resistance of the oxide film is an indicator of corrosion inhibiting behavior. As shown in Fig. 3 the average impedance of the films grown from ozone is ~10 times higher than that for oxygen-grown films with a similar thickness (15–16 Å). Direct current measurements also showed an increased corrosion passivating property for oxide layers grown with ozone. The corrosion current density for ozone-formed oxide is 4.5 times lower than for oxygen-formed films. The pitting potential is higher by 44 mV for the ozone-formed layer.

As measured by Auger spectroscopy, the dramatic increase in exposure to oxygen due to atmospheric exposure after the samples are removed from the vacuum chamber causes an increase in the O(*KLL*) Auger intensity. This is postulated to be due to additional oxidation of both ozone- and oxygen-formed films. The corrosion passivation properties of the film measured by EIS and Tafel analysis, after atmospheric exposure on nine samples originally oxidized with O_3, consistently showed higher impedance and smaller values of the corrosion rate. Evidently, the structural and electrical properties of the thin 15 Å film of the O_3-grown oxide render improved stability towards corrosion even after a dramatic increase in exposure to oxygen in the atmosphere.

D. Open circuit potential measurements and relation between solid state and electrochemical measurements

More positive open circuit potential values were observed for ozone- formed oxide in 3.5% NaCl solution compared to oxygen-formed oxide film. The more positive open circuit potential results when the oxide is more resistant to electron transport (less conductive). Because the oxide electrochemical properties are dependent on the rate of electron transport across the oxide, the solid state and electrochemical properties are correlated. A diagram of the potential difference between the reference electrode and the working electrode (aluminum sample) is shown in Fig. 7. The average measured potential difference is −1.40 V for oxygen-formed oxide and −1.17 for ozone-formed oxide. The higher OCP corresponds to a higher value of the work function, φ. The structural and electronic effects governing corrosion kinetics may be related to the differences in work function observed through the OCP measurements.

V. CONCLUSIONS

A number of interesting conclusions can be drawn from this study of the oxidation of Al(111) and polycrystalline Al.

(1) The initial kinetics of formation of the oxide layer are faster for O_3 than for O_2 on both Al(111) and polycrystalline Al. This is attributed to the more favorable thermodynamic energy of ozone compared to oxygen.

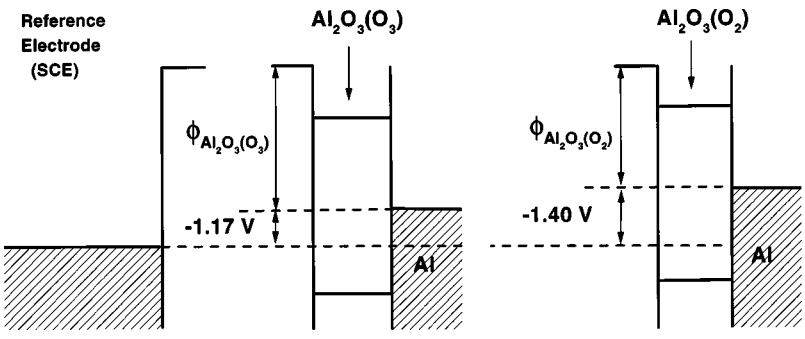

FIG. 7. Open circuit potential between the reference electrode and the aluminum sample.

(2) Ozone-grown films exhibit about 10 times higher electrical impedance compared to O_2-grown films of similar thickness. This observation is attributed to a more effective oxide barrier layer produced by O_3 compared to that by O_2.
(3) Ozone-grown films exhibit a lower critical corrosion current density compared to O_2-grown films measured by the Tafel method.
(4) Ozone-grown films exhibit a 4% higher average density compared to O_2-grown films. This is postulated to be due to the reduction of oxygen vacancy sites in oxide films grown from O_3.
(5) Ozone-grown films exhibit a slightly higher pitting potential compared to oxygen-grown films.
(6) A more positive value for the open circuit potential is found for ozone-grown films compared to oxygen-grown films.
(7) The special electrical properties of ozone-grown films are preserved even when the films are exposed to the atmosphere and undergo significant additional oxidation. This suggests that the special properties of the ozone-grown films are not appreciably altered by subsequent oxidation by O_2 under extreme conditions of exposure.

ACKNOWLEDGMENTS

The authors acknowledge with gratitude the support of the Air Force Office of Scientific Research and the National Science Foundation. They thank Dr. T. Nuhfer for his assistance with the TEM.

[1]H. D. Ebinger and J. T. Yates, Jr., Phys. Rev. B **57**, 1976 (1998).
[2]A. Kuznetsova, T. D. Burleigh, V. Zhukov, and J. T. Yates, Jr., Langmuir **14**, 2502 (1998).
[3]I. Popova, V. Zhukov, and J. T. Yates, Jr., Langmuir (accepted).
[4]J. T. Yates, *Experimental Innovations in Surface Science* (Springer, New York, 1998), p. 702.
[5]V. Zhukov, I. Popova, and J. T. Yates, Jr., J. Vac. Sci. Technol. A **18**, 992 (2000).
[6]A. Winkler and J. T. Yates, Jr., J. Vac. Sci. Technol. A **6**, 2929 (1988).
[7]S. R. Elliott, *Physics of Amorphous Materials*, 2nd ed. (Wiley, New York, 1990).
[8]W. S. Tait, *An Introduction to Electrochemical Corrosion Testing for Practicing Engineers and Scientists* (PairODocs, Racine, WI, 1994), p. 109.
[9a]H. Brune, J. Wintterlin, J. Trost, G. Ertl, J. Wiechers, and R. J. Behm, J. Chem. Phys. **99**, 2128 (1993).
[9b]V. Zhokov, I. Popova, and J. T. Yates, Jr., Surf. Sci. **441**, 251 (1999).
[10]N. A. Saliba, Y.-L. Tsai, and B. E. Koel, J. Phys. Chem. B **103**, 1532 (1999).
[11]F. De Smedt, C. Vinckier, I. Cornelissen, S. De Gendt, and M. Heyns, J. Electrochem. Soc. **147**, 1124 (2000).
[12]S. W. Benson, *Thermodynamical Kinetics* (Wiley, New York, 1996).
[13]F. P. Felhner and N. F. Mott, Oxid. Met. **2**, 59 (1970).